Facile synthesis of highly stable and well-dispersed mesoporous ZrO_2/carbon composites with high performance in oxidative dehydrogenation of ethylbenzene†

Qiang Li, Jie Xu, Zhangxiong Wu, Dan Feng, Jianping Yang, Jing Wei, Qingling Wu, Bo Tu, Yong Cao and Dongyuan Zhao*

Received 19th March 2010, Accepted 14th May 2010
DOI: 10.1039/c004469e

Highly ordered mesoporous ZrO_2/carbon (FDU-15) composites have been synthesized *via* a facile evaporation induced triconstituent co-assembly (EISA) approach by using Pluronic F127 as a template and zirconium oxychloride octahydrate and resol as Zr and carbon sources. The synthesized mesoporous composites exhibit a highly ordered two-dimensional (2-D) hexagonal mesostructure with relatively high specific surface areas (up to 947 $m^2\ g^{-1}$), pore sizes around 3.8 nm and high pore volumes (up to 0.71 $cm^3\ g^{-1}$). The results clearly show that the crystalline zirconia nanoparticles (*ca.* 1.9–3.9 nm) are well-dispersed in amorphous matrices of the ordered mesoporous carbon FDU-15 materials, which construct the nanocomposites. The ordered mesostructures of the obtained ZrO_2/FDU-15 composites can be well-retained even at the high pyrolysis temperature (up to 900 °C), suggesting a high thermal stability. The zirconia content of the ZrO_2/FDU-15 composites can be tunable in a wide range (up to 47%). Moreover, the resultant mesoporous ZrO_2/FDU-15 composites exhibit high catalytic activity in oxidative dehydrogenation (ODH) of ethylbenzene (EB) to styrene (ST), with high ethylbenzene conversion (59.6%) and styrene selectivity (90.4%), which is mainly attributed to the synergistic catalytic effect between the oxygen-containing groups located on the carbon pore walls and weakly basic sites of the nanocrystalline ZrO_2. Furthermore, the high specific surface areas and opening pore channels are also responsible for their high catalytic activity. Therefore, it is a very promising catalyst material in styrene production on an industrial scale.

1. Introduction

In recent years, zirconia has received great attention owing to its extensive applications in many areas, such as gas sensors,[1,2] solid oxide fuel cells (SOFCs),[3] and automotive exhaust three-way catalysts,[4,5] especial acid–base bifunctional catalysts.[6,7] However, the relatively low specific surface area ($<100\ m^2\ g^{-1}$) and microporosity for bulk zirconia limit its applications. A large number of researchers have focused on the preparation of porous zirconia with high specific surface area and uniform pore channels by using ionic or nonionic surfactants as structure-directing agents.[8–10] For instance, Shi *et al.* synthesized mesoporous phosphated zirconia by a hydrothermal method, where cetyltrimethylammonium bromide (CTAB) and zirconium sulfate were used as a structure-directing agent and precursor, respectively.[10] Unfortunately, the mesoporous zirconia usually has poor thermal stability, and it has been shown that the mesostructure completely collapses after being calcined at a high temperature (above 500 °C).[11] Simultaneously, the surface area drastically decreases after the high temperature treatment.

To improve the thermal stability and specific surface areas, many researchers focused on supporting zirconia on high-surface-area mesoporous silica by direct-[12–14] or post-synthesis[15–17] methods. For instance, Chen *et al.* synthesized ordered mesoporous sulfated zirconia/silica composites by a direct-synthesis method using triblock copolymer Pluronic P123 as a template, and zirconium propoxide and tetraethyl orthosilicate (TEOS) as precursors, respectively.[14] Moreover, Landau *et al.* synthesized sulfated ZrO_2/SBA-15 catalysts from a chemical solution decomposition (CSD) method (post-synthesis) by calcination at 500–600 °C.[16] However, there are still some drawbacks that cannot be conquered by the two synthesis strategies. On the one hand, the mesoporous zirconia/silica composites synthesized by a one-pot method usually have low zirconia content[12,13] or inhomogeneous zirconia distribution and particle size.[14] On the other hand, pore blocking normally cannot be avoided for zirconia/silica composites with a high zirconia content. Generally, success in supporting metal oxides on mesoporous materials requires not only high loadings (>30 wt%)[15] for obtaining high active materials but also minimal pore blocking for getting high surface areas and opening pore channels.

In addition, compared with mesoporous silica, carbon materials, such as the FDU series templated by triblock

Department of Chemistry and Shanghai Key Laboratory of Molecular Catalysis and Innovative Materials, Laboratory of Advanced Materials, Fudan University, Shanghai, 200433, People's Republic of China. E-mail: dyzhao@fudan.edu.cn; Fax: +86-21-5163-0307; Tel: +86-21-5163-0205

† Electronic supplementary information (ESI) available: Fig. S1–S5. See DOI: 10.1039/c004469e

copolymers PEO-PPO-PEO from the direct organic–organic assembly method,[18–20] have higher thermal stability (above 1500 °C) and more easily functionalized pore walls, which show great potential in their uses, such as catalysts and catalyst supports, biosensors, adsorption, *etc*.[21–23] Because of the functionality of zirconia materials, the combination of zirconia and mesoporous carbon could exhibit many unique properties in many research fields, such as catalysis, sensors, electrochemistry, and so on. Moreover, the synthesis of mesoporous ZrO_2/C composites may be another effective way to improve the thermal stability and specific surface areas of ZrO_2 materials. However, to the best of our knowledge, no paper related to the synthesis and application of zirconia/mesoporous carbon materials has been reported until now.

Herein, we report for the first time a facile synthesis of highly thermally stable (up to 900 °C) mesoporous ZrO_2/FDU-15 composites with ordered 2-D hexagonal mesostructures *via* an EISA strategy by using the simple inorganic salt $ZrOCl_2{\cdot}8H_2O$ and resol as the zirconium and carbon source, respectively, and Pluronic F127 as a template. The synthesized ZrO_2/carbon composites with high BET surface areas (up to 947 $m^2\ g^{-1}$) have adjustable zirconia content (up to 47 wt%). Nanocrystalline ZrO_2 particles are well-dispersed in the mesoporous carbonaceous frameworks. The degree of pore blocking is very small despite the high embedded amount of zirconia (> 30 wt%) in the amorphous carbon matrices. Moreover, the ordered mesoporous ZrO_2/FDU-15 composites exhibit high catalytic activity for the oxidative dehydrogenation of ethylbenzene to styrene, with high ethylbenzene conversion (59.6%) and styrene selectivity (90.4%).

2. Experimental

2.1 Chemicals

Triblock copolymer poly(ethylene oxide)-*b*-poly(propylene oxide)-*b*-poly(ethylene oxide) Pluronic F127 ($EO_{106}PO_{70}EO_{106}$, M_{av} = 12 600 g mol^{-1}) was purchased from Aldrich Chemical Inc. Phenol, formalin (37 wt%), absolute ethanol and $ZrOCl_2{\cdot}8H_2O$ were purchased from Shanghai Chemical Co. All chemicals were used as received without any further purification. Millipore water was used in all experiments.

1.2 Synthesis of resol precursor

The resol precursor solution used as a carbon source was prepared according to the method reported previously under basic conditions.[19] Typical preparation procedure could be described as follows: phenol (6.1 g, 65 mmol) was melted at 40–42 °C before 20 wt% NaOH (aq; 1.3 g, 6.5 mmol) was added slowly with stirring. Formalin (37 wt%, 10.5 g) containing formaldehyde (130 mmol) was added dropwise, and the reaction mixture was stirred at 70 °C for 1 h. After cooling the mixture to room temperature, the pH value of the reaction mixture was adjusted to neutral (7.0) by using (0.60 M) HCl aqueous solution. Water was then removed under vacuum below 50 °C. The final product was re-dissolved in ethanol before use.

2.3 Synthesis of zirconia–carbon composites

The mesoporous ZrO_2/FDU-15 composites were synthesized by using zirconium oxychloride octahydrate and resol as precursors and Pluronic F127 as a template under the EISA approach. In a typical synthesis procedure, 1.5 g of triblock copolymer Pluronic F127 was dissolved in 30 g of ethanol. Then 0.6 g of zirconium oxychloride octahydrate was added into the above solution. The mixture solution was stirred at room temperature for 15 min to dissolve the zirconium salt. Then the resol precursors in ethanol solution containing phenol (0.92 g, 9.72 mmol) and formaldehyde (0.58 g, 19.44 mmol) were added with stirring for 10 min to form a homogeneous solution with a molar composition of F127/phenol/formaldehyde/zirconium source/ethanol of 0.012 : 1 : 2 : 0.19 : 67. The solution was transferred to a dish and the ethanol evaporated at room temperature for 5–8 h to produce a transparent membrane. The membrane was then heated in an oven at 100 °C for 24 h to get the as-made sample. The product (denoted as ZC-I-as-made) was peeled off and pyrolyzed at different temperatures under a nitrogen flow (60 mL min^{-1}). The ramping rate was 1 °C min^{-1} below 600 °C, and 2 °C min^{-1} above 600 °C; pyrolysis was suspended at 350 °C for 2 h, and at the final temperature for 2 h (denoted as ZC-I-X, where X represents for the final pyrolysis temperature). Sample ZC-II-X, ZC-III-X and ZC-IV-X were synthesized according to the above experimental procedure, except the amount of zirconium oxychloride octahydrate was increased to 0.9, 1.2, and 1.5 g, respectively.

2.4 Synthesis of mesoporous zirconia and carbon FDU-15

For a control experiment, mesoporous carbon FDU-15 and mesoporous zirconia (meso-ZrO_2) were synthesized by the following strategies: mesoporous carbon FDU-15 was synthesized according to the method reported previously,[19] except the pyrolysis process of the as-made sample under nitrogen atmosphere was instead carried out by heating at 350 °C for 2 h, and then at 600 °C for 2 h with a ramping rate of 1 °C min^{-1}. The meso-ZrO_2 sample was prepared by using a hard template approach (nanocasting). The experimental procedure was carried out as follows: 0.4 g of zirconium oxychloride octahydrate was dissolved in 6.0 g of ethanol. Then, 0.15 g of mesoporous slica SBA-15 obtained according to the previous method[24] was added into the ethanol solution. After stirring for 2 h at room temperature, the ethanol solvent was evaporated by heating at 40 °C to get the as-made product (I). After being calcined at 300 °C for 3 h in air, the composite product (I) (ZrO_2/SBA-15) was filled again using 0.3 g of zirconium oxychloride octahydrate by the same procedure mentioned above. Then, the final as-made product (II) was calcined at 500 °C for 4 h in air to get the ZrO_2/SBA-15 composite (II). Finally, this calcined sample was treated by using (2 M) NaOH at 70 °C for 24 h to get mesoporous zirconia (meso-ZrO_2).

2.5 Characterization

Small angle X-ray scattering (SAXS) measurements were carried out on a NanoSTAR small-angle X-ray scattering system (Bruker, Germany) using Cu-Kα radiation (40 kV, 35 mA).

The *d*-spacing values were calculated by the formula $d = 2\pi/q$, and the unit cell parameters were calculated from the formula $a = 2d_{10}/\sqrt{3}$. Wide-angle X-ray diffraction (WAXRD) patterns were collected on a Bruker D4 Endeavor X-ray diffractometer using CuKα radiation (40 kV, 40 mA). Transmission electron microscopy (TEM) images and energy-dispersive X-ray spectroscopy (EDXS) were recorded on a JEOL 2100F microscope operated at 200 kV. Before the TEM characterization, the samples were dispersed in ethanol. The suspensions of the samples were dropped on a holey carbon coated copper grid. Thermogravimetric (TG) analysis was carried out on a Mettler Toledo TGA-SDTA851 analyzer (Switzerland) from 25 to 900 °C in an air flow of 80 mL min^{-1} at a heating rate of 10 °C min^{-1}. Nitrogen sorption isotherms were measured with a Micromeritics Tristar3000 (USA) analyzer at 77 K. Before measurements, the samples were degassed at 180 °C in a vacuum for more than 6 h. The Brunauer–Emmett–Teller (BET) method was utilized to calculate the specific surface areas (S_{BET}). The pore size distributions were calculated by using the Barrett–Joyner–Halenda (BJH) model from the adsorption branches of isotherms. The total pore volumes (V_t) were estimated from the adsorbed amount at a relative pressure P/P_0 of 0.99. FT-IR spectra of the samples were measured on a Nicolet FT-IR360 spectrometer *via* the usual KBr pellet technique.

2.6 Catalytic test

The oxidative dehydrogenation (ODH) of ethylbenzene (EB) to styrene (ST) reaction was carried out in a quartz tube reactor (5 mm i.d. × 500 mm) at 350 °C under atmospheric pressure. In a typical test, 50 mg of catalyst was held between two quartz wool plugs in the isothermal zone. The reactant was a flowing mixture with 2.4 vol% EB (O_2/EB ratio of 0.5, nitrogen as the dilutent), and the total space velocity (SV) was 24 900 mL g^{-1} h^{-1}. To investigate the stability of the catalyst, the catalytic reaction was firstly sustained for 120 min. After that, the flowing gas was switched into pure nitrogen, and the catalyst was swept for half an hour at 350 °C. Then, the catalyst was reused for 120 min under the same reaction condition (Reuse 1). After that, it was repeated again (Reuse 2). The products were analyzed by an on-line gas chromatograph (Agilent GC 6820 equipped with FFAP column for hydrocarbons and TDX-01 column for permanent gas analysis, coupled with FID and TCD detectors respectively).

3. Results and discussion

3.1 Structural and textural properties of mesoporous ZrO_2/FDU-15 composites

The mesoporous ZrO_2/FDU-15 composites can be synthesized from the EISA of Pluronic F127, resol and zirconium oxychloride octahydrate, followed by thermal curing and pyrolysis in nitrogen. The SAXS pattern of the as-made mesoporous hybrid polymer/Zr composite (ZC-I-as-made) displays two scattering peaks, which may be indexed as the 10, and 11 reflections of ordered hexagonal mesostructure with *p6mm* space group (Fig. 1a). The cell parameter (a_0) is calculated to be ~15.7 nm. After being pyrolyzed at 600 °C, the ordered hexagonal mesostructure of ZC-I-600 is well retained (Fig. 1b), as the 10 scattering peak shifts to a high *q*-value, suggesting a shrinkage (32%) of the cell parameter (a_0 = 10.6 nm). Moreover, the 11 scattering peak becomes relatively more resolved, arising from the increase of contrast between the mesopores and pore walls. With the increase of the pyrolysis temperature, the mesostructural shrinkage becomes very small (Table 1), owing to the improvement of the rigidity of the carbon matrix. The SAXS pattern of the mesoporous ZrO_2/FDU-15 composite (ZC-I-900) pyrolyzed at 900 °C becomes a little poorly resolved (Fig. 1e), suggesting that the ordered mesostructure is retained. These results clearly suggest that the mesoporous ZrO_2/FDU-15 composite is highly thermally stable. With the increase of zirconia content (for the samples ZC-I-600 to ZC-IV-600), SAXS patterns still exhibit an ordered hexagonal mesostructure (Fig. 1f–i), suggesting a high thermal stability. However, after being pyrolyzed at 900 °C, the SAXS patterns of mesoporous ZrO_2/FDU-15 composites (especially for ZC-IV-900) become more poorly resolved, suggesting that the mesostructure gradually degenerates. It is related to the growth of zirconia nanoparticles embedded in the amorphous carbon matrix (Fig. S1 in the ESI†).

The WAXRD pattern of mesoporous ZrO_2/FDU-15 composite pyrolyzed at 900 °C (ZC-I-900) (Fig. 2A) shows four wide diffraction peaks which can be indexed to be the 101, 110, 112, 211 reflections of the tetragonal zirconia phase, according to the Joint Committee for Powder Diffraction Studies (JCPDS, card number 79-1766). The small diffraction peak at around 22.6° (marked with an asterisk in Fig. 2) can be assigned to the amorphous carbon. These results clearly indicate that the zirconia nanocrystals with tetragonal

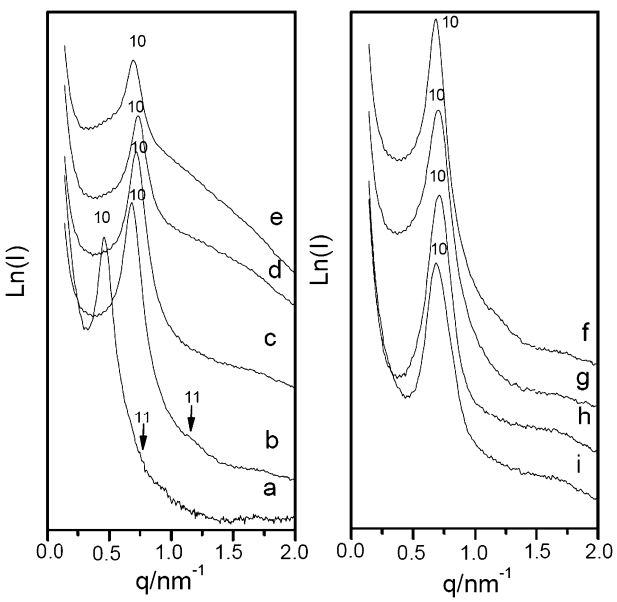

Fig. 1 SAXS patterns of the ordered mesostructured ZC-I-as-made polymers and the corresponding mesoporous zirconia/FDU-15 composites with different zirconium contents and pyrolysis temperatures: (a) ZC-I-as-made; (b) ZC-I-600; (c) ZC-I-700; (d) ZC-I-800; (e) ZC-I-900; (f) ZC-I-600; (g) ZC-II-600; (h) ZC-III-600; and (i) ZC-IV-600. See Experimental for details on the sample designations.

Table 1 Textural properties of ordered mesoporous zirconia/FDU-15 composites

Sample number	d_{100} spacing/nm	Unit cell size/nm	Pore size/nm	Pore wall thickness/nm	Pore volume/ $cm^3\ g^{-1}$	BET surface area/$m^2\ g^{-1}$	ZrO_2 content[a] (wt%)
ZC-I-as-made	13.6	15.7	—	—	—	—	—
ZC-I-600	9.2	10.6	3.8	6.8	0.27	318	31
ZC-I-700	8.7	10.0	3.8	6.2	0.36	498	36
ZC-I-800	8.6	9.9	3.8	6.1	0.71	910	37
ZC-I-900	9.0	10.4	3.8	6.6	0.56	947	44
ZC-II-600	9.0	10.4	3.8	6.6	0.24	328	38
ZC-III-600	8.9	10.3	3.5	6.8	0.28	332	42
ZC-IV-600	9.2	10.6	3.2	7.4	0.26	315	47

[a] ZrO_2 contents were determined by TG measurements under air flow of 80 mL min^{-1}.

structure are formed during the pyrolysis process at high temperature (900 °C). Furthermore, with the decrease of the pyrolysis temperature, the broadening effect of the diffraction peaks becomes more obvious, suggesting that the particle size of the zirconia nanocrystals decreases gradually (Fig. 2A). Estimated from the diffraction peaks by the Scherrer equation, the sizes of the ZrO_2 nanocrystals are 1.9, 2.9, 3.1, and 3.9 nm for sample ZC-I-600, ZC-I-700, ZC-I-800, and ZC-I-900, respectively, suggesting an increase with the pyrolysis temperatures. Furthermore, we found that the particle sizes are not only related to the pyrolysis temperature, but also with the ZrO_2 content in the mesoporous composites. As the content increases, the zirconia particle sizes gradually increase, as shown in Fig. 2B, because the higher the zirconia concentration is, the more easily it aggregates into large particles during the pyrolysis process.

TEM images (Fig. 3a and b) of the mesoporous ZrO_2/FDU-15 composite ZC-I-600 show a well-defined 2-D hexagonal mesostructure, which is consistent with that of the SAXS pattern (Fig. 1b). The zirconia nanoparticles are homogenously embedded in the carbonaceous matrix. The homogeneous dispersion of zirconium can be confirmed from the element mapping in energy dispersive X-ray spectroscopy (EDXS) measurements (Fig. 3c and d). After being further pyrolyzed at 900 °C in nitrogen atmosphere, the hexagonal mesostructure of sample ZC-I-900 is retained (Fig. 4). High-resolution TEM (HRTEM) analysis reveals that the characteristic lattice fringes (marked with circles in Fig. 4b) of the zirconia nanocrystals are observed with random orientation in the high-contrast areas of carbon pore walls. The diffusive selected area electron diffraction (SAED) pattern (Fig. 4b, inset) further confirms the formation of nanocrystalline ZrO_2 with a tetragonal structure, which undergoes a high dispersion in the amorphous carbon matrix. The particle size of ZrO_2 nanocrystals is measured to be around 4 nm, in agreement with that calculated from WAXRD measurements. With the increase of zirconia content (from sample ZC-II-600 to ZC-IV-600), large domains of ordered hexagonal arrays are observed by TEM analysis (Fig. S2†). Furthermore, it is also found that the ZrO_2 nanoparticles gradually become larger with the increase of the ZrO_2 content from the TEM images (Fig. S2†), which is consistent with the results of WAXRD patterns (Fig. 2B). According to the above TEM observations, the zirconium species are highly dispersed in the carbonaceous frameworks during the co-assembly of the mesostructures, and a large number of ZrO_2 nanocrystals could be formed in the amorphous carbon matrices during the pyrolysis.

Compared with the nitrogen sorption isotherm of pristine FDU-15 (Fig. S3b in the ESI†), mesoporous ZC-I-600 composites still exhibit representative type IV curves with H_2 hysteresis

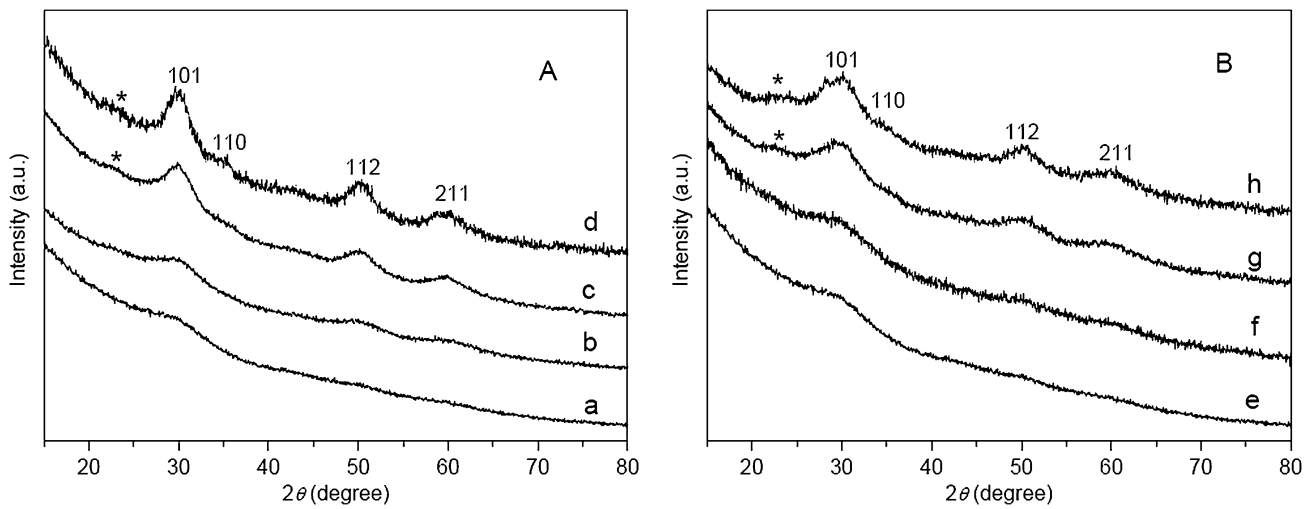

Fig. 2 Wide-angle XRD patterns of (A) the mesoporous ZC-I-X composites pyrolysized at different temperatures and (B) mesoporous ZrO_2/FDU-15 composites with different zirconia content. (a) ZC-I-600; (b) ZC-I-700; (c) ZC-I-800; and (d) ZC-I-900; (e) ZC-I-600; (f) ZC-II-600; (g) ZC-III-600; and (h) ZC-IV-600.

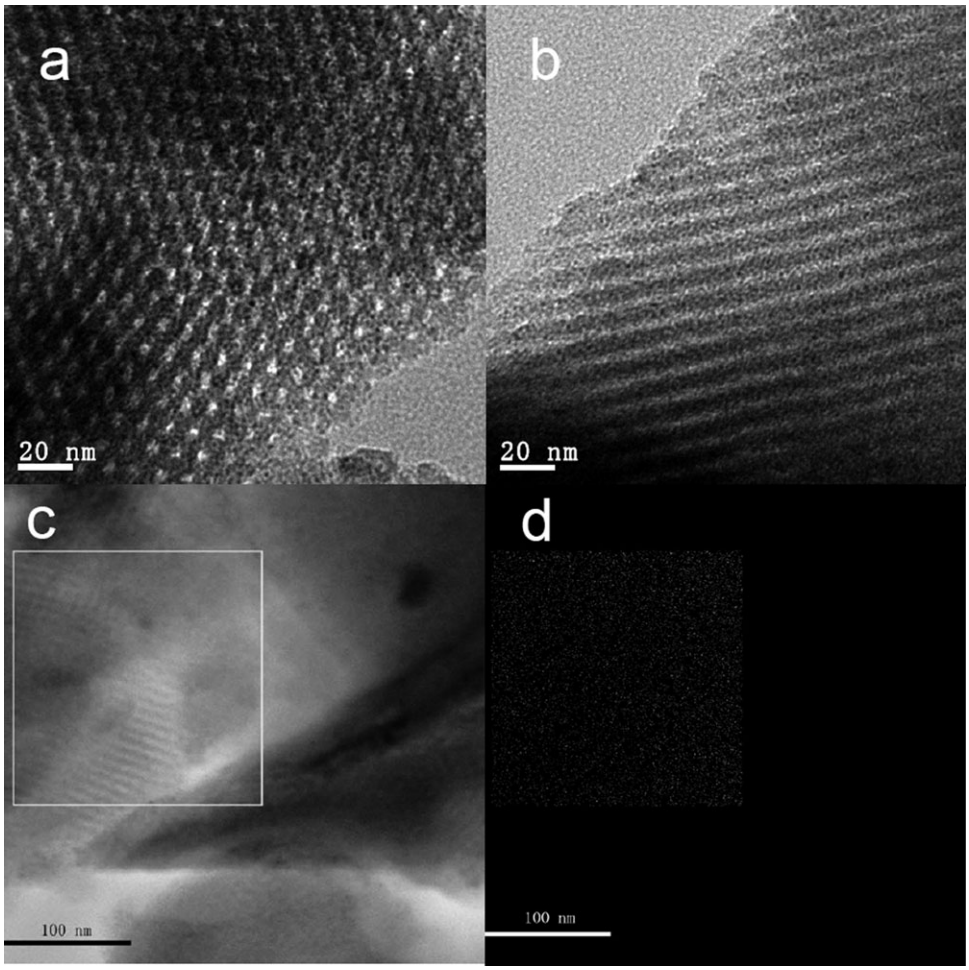

Fig. 3 TEM images (a, b, c) and energy dispersive X-ray (EDX) mapping (d) of mesoporous ZrO_2/FDU-15 composites (ZC-I-600). The images were taken along (a) the [001] and (b) [110] directions, respectively. (c) Low magnification TEM image, showing high ordering of this material in large domains. (d) The corresponding zirconium element face mapping (marked with rectangle in Fig. 3c), showing the high dispersion of zirconium in the carbon matrices.

loop (Fig. 5Aa), which suggest the introduction of zirconia nanoparticles does not obviously affect the porous mesostructure. A clear capillary condensation is observed at a relative pressure (P/P_0) of 0.4–0.55, indicating a narrow pore size distribution (Fig. 5Aa and Ca). The mean pore size of sample ZC-I-600 is around 3.8 nm. With the increase of the zirconia content (from sample ZC-I-600 to ZC-IV-600), the pore size decreases from 3.8 to 3.2 nm, due to large zirconia nanocrystals in the cylinder mesopores. Interestingly, the pore sizes of the mesoporous ZC-I-X composites are changeless with the enhancement of the pyrolysis temperature (Fig. 5D and Table 1). Therefore, the pore blocking seemingly can be avoided by using this facile triconstituent co-assembly method. Simultaneously, the specific BET surface area of the sample ZC-I-X increases from 318 to 910 $m^2\ g^{-1}$, with the increase of pyrolysis temperature, because more micropores are generated. Furthermore, the pore wall thickness of the mesoporous ZrO_2/FDU-15 composites is calculated to be in the range of 6.1–7.4 nm, which is larger than the particle sizes of zirconia nanocrystals (<4 nm) estimated from WAXRD and HRTEM. Therefore, it agrees well with the observations that nanocrystalline ZrO_2 particles are embedded in the amorphous carbon pore walls.

With the increase of zirconium oxychloride octahydrate in the synthesis processes, TG analyses (Fig. S5 in ESI†) show that the zirconia contents correspondingly increase in the mesoporous ZrO_2/FDU-15 composites. The weight percents of zirconia are 31, 38, 42, and 47 wt% for the samples ZC-I-600, ZC-II-600, ZC-III-600, and ZC-IV-600, respectively (Table 1). Furthermore, it is found that the increase of the pyrolysis temperature can give higher zirconia content. For example, for sample ZC-I-X, increasing the temperature from 600 to 900 °C, the zirconia content increases from 31 to 44 wt%, owing to more small molecules generated at higher pyrolysis temperature, such as CO_2, H_2O, *etc*. Therefore, these results suggest that a large amount of zirconia can be incorporated in frameworks of the ordered mesoporous carbons.

3.2 The formation mechanism of mesoporous ZrO_2/FDU-15 composites

On the basis of the above observations, we speculate that the mesoporous ZrO_2/FDU-15 composites are formed by the

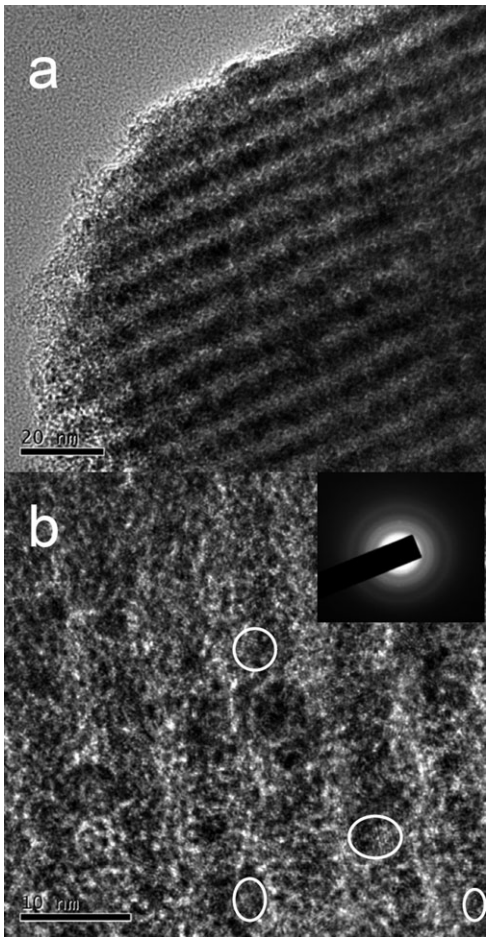

Fig. 4 (a) TEM image of the mesoporous ZrO_2/FDU-15 composite ZC-I-900 after being pyrolyzed at 900 °C taken along the [110] direction; and (b) the corresponding HRTEM image.

EISA[25] of organic polymer resol, zirconium polyoxo oligomers hydrolyzed from zirconium oxychloride octahydrates[14] and amphiphilic Pluronic F127. When zirconium oxychloride ($ZrOCl_2$) is added into Pluronic F127 ethanol solution, it can hydrolyze with structural water and ethanol, and yield zirconium polyoxo oligomers.[14] The resol precursor is preformed from phenol and formaldehyde under alkaline conditions, therefore, it has a 3-D network structure with benzene ring as three- or four-linking sites.[25,26] As a result, the resol together with the zirconium polyoxo oligomers can interact with Pluronic F127 templates by the hydrogen-bonding.[18–20] Therefore, under the assistance of the resol precursor, during the ethanol evaporation the co-assembly of these species, F127–resol–zirconium polyoxo oligomers, can occur. In the curing process at 100 °C, the cross-linkage of the resol oligomers occurs, therefore, the 3-D network becomes more rigid and robust. Simultaneously, the zirconium polyoxo species is further polymerized. During the pyrolysis process, the zirconia nanocrystals with uniform size (<4 nm) are formed. Because of the homogenous distribution of zirconium polyoxo species in the 3-D network, the ZrO_2 nanoparticles are homogenously confined in the carbonaceous frameworks.

3.3 The catalytic performance of mesoporous ZrO_2/FDU-15 composites

Styrene (ST) is an important monomer extensively used in the chemical industry for the manufacture of polymers, copolymers, and reinforced plastics.[27] In a practical industrial process, styrene is usually produced by the direct dehydrogenation of ethylbenzene (EB) at high reaction temperature (600–650 °C) over K-promoted iron oxide catalyst in the presence of a large quantity of steam.[28] However, this method is thermodynamically limited and, because of the required excess of steam, very energy consuming.[29] The oxidative dehydrogenation of ethylbenzene to styrene has attracted considerable attention owing to the absence of detrimental thermodynamic limitations and lower operation temperatures. A range of catalysts have been reported for this process including amorphous $AlPO_4$, carbon materials, zirconia, *etc*.[30–35] The results show differently structural carbon materials exhibit good catalytic performance, such as onion like carbon (OLC)[36] and carbon nanofibers (CNF)[32] at *ca*. 400–500 °C. Presumably, higher temperature as well as a higher molar ratio of O_2/EB should give rise to better catalytic activity. However, considering the intrinsic property of the low resistance to combustion of the carbon nanomaterials and the deep oxidation of feedstocks, higher reaction temperature and molar ratios of O_2/EB (≥ 1.0) are not favorable. In this context, there is a great incentive to develop a new robust catalyst applicable for the oxidative dehydrogenation of ethylbenzene at low reaction temperature along with low O_2/EB molar ratios.

The mesoporous ZC-I-600 composite exhibits excellent catalytic performance toward the oxidative dehydrogenation of ethylbenzene even at relatively low temperature (350 °C) and low O_2/EB molar ratio (O_2/EB = 0.5). It has high styrene selectivity (90.4%) and ethylbenzene conversion (59.6%) after the reaction is sustained for 60 min, which is superior to other typical catalysts (Table 2), such as microporous carbons, carbon nanotubes, $AlPO_4$, *etc*. Furthermore, after the catalyst was reused for twice, the ethylbenzene conversion (56.1%) and styrene selectivity (90.2%) show only a minor change (Table 2). It suggests that the catalytic activity of this material is very stable for the oxidative dehydrogenation of ethylbenzene. In this catalytic reaction, the low reaction temperature is helpful for high styrene selectivity and lowering the energy consumption. The low O_2/EB ratio can avoid the deep oxidation to some extent. In addition, the low reaction temperature and oxygen content in the feedstock are also favorable for the mesostructural stability and resistance to combustion of the mesoporous composite.

For comparison, mesoporous carbon FDU-15 and mesoporous zirconia were synthesized. The corresponding textural properties are shown in Fig. S3 of the ESI†. The catalytic results show pristine FDU-15 also exhibits relatively high catalytic activity (Table 2) with a styrene selectivity of 95.6% and ethylbenzene conversion of 47.0%, because plentiful oxygen-containing groups are located on the pore wall, confirmed by the corresponding FT-IR spectrum (Fig. S4 in the ESI†). It has three obvious bands at 3442, 1612, and 1100 cm^{-1}, arising from vibrational stretching of –OH, C=C and C–O groups, respectively. These groups are the

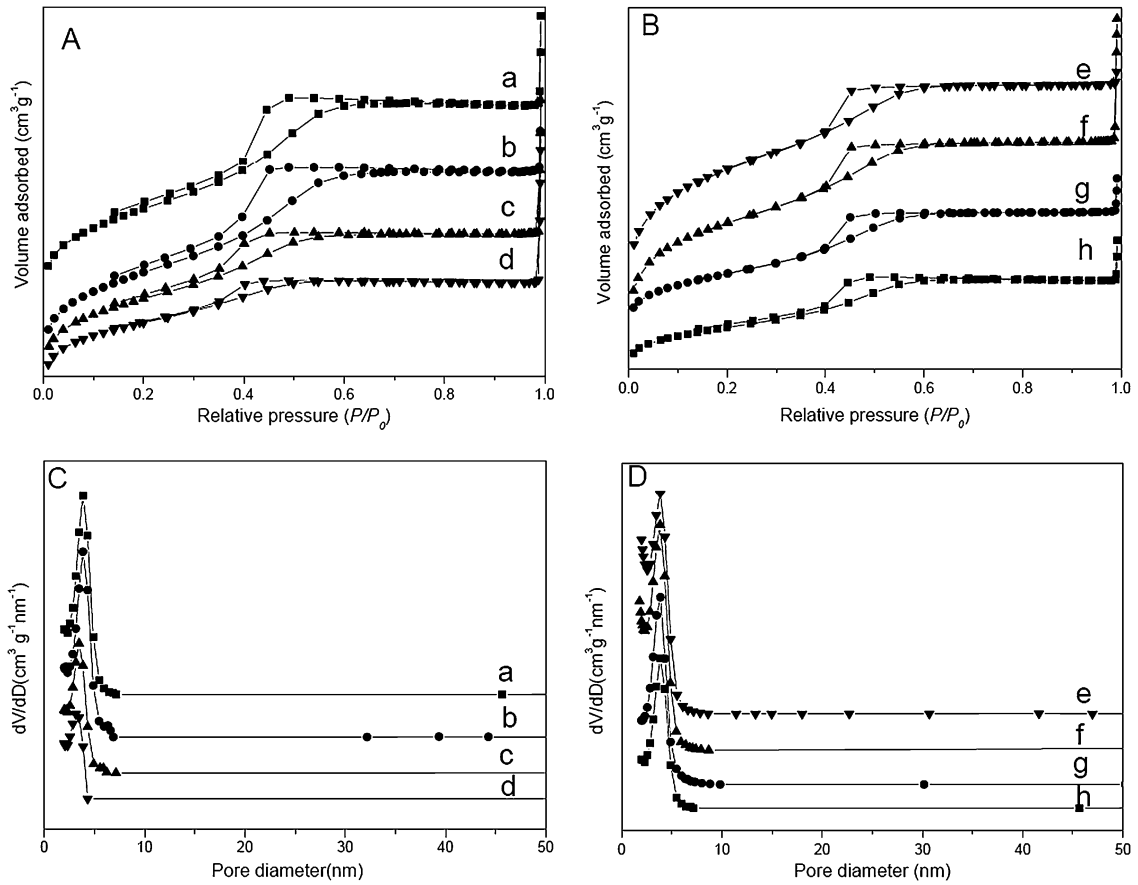

Fig. 5 Nitrogen sorption isotherms (A and B) and corresponding pore size distributions (C and D) of the mesoporous ZrO_2/FDU-15 composites with different zirconia content and pyrolysis temperatures. (a) ZC-I-600; (b) ZC-II-600; (c) ZC-III-600; (d) ZC-IV-600; (e) ZC-I-900; (f) ZC-I-800; (g) ZC-I-700; and (h) ZC-I-600.

Table 2 Catalytic activities of different catalysts for the oxidative dehydrogenation of ethylbenzene

Catalyst	O_2/EB ratio	SV[a]/mL g^{-1} h^{-1}	T^b/°C	EB conversion (%)	ST selectivity (%)	Reaction rate[c] (mmol-ST g^{-1} h^{-1})
ZC-I-600[d]	0.5	24 900	350	59.6	90.4	14.4
ZC-I-600 (Reuse 1)[d]	0.5	24 900	350	57.5	90.5	13.9
ZC-I-600 (Reuse 2)[d]	0.5	24 900	350	56.1	90.2	14.0
FDU-15[d]	0.5	24 900	350	47.0	95.6	12.0
Meso-ZrO_2[d]	0.5	24 900	350	3.0	20.6	0.17
ZrO_2[30]	1	3636	440	5.2	94.0	0.04
popcarbon-900[31]	1	12 000	400	48.0	86.0	6.2
carbon nanofibers[32]	5	5000	400	28.0	80.0	1.0
CNTs/bentonite[33]	2.5	22 959	400	49.0	60.0	8.6
CNT3[34]	1	8500	400	43.0	67.0	2.7
$AlPO_4$[30]	1	3636	440	43.5	99.7	0.35

[a] The total space velocity. [b] Reaction temperature. [c] Reaction rate obtained after reaction for 60 min. [d] Reaction condition: 50 mg catalyst, the catalytic results were acquired after the reaction lasted for 60 min.

active sites for the oxidative dehydrogenation of ethylbenzene.[28,36] Furthermore, it is possible that more oxygen-containing groups are formed in the reaction process because of the existence of oxygen as oxidant.[36] However, the mesoporous zirconia (meso-ZrO_2) exhibits poor catalytic performance in these reaction conditions. Interestingly, after the incorporation of ZrO_2 nanoparticles into the carbonaceous frameworks, the styrene yield further increases from 44.9% for pristine FDU-15 to 53.9% for mesoporous composite (ZC-I-600). As reported in the literature,[35–37] tetragonal ZrO_2 nanoparticles have abundant weak basic sites which are favorable for the oxidative dehydrogenation process. The excellent catalytic performance of the ordered mesoporous ZC-I-600 composite may be mainly contributed from the synergetic interaction between the oxygen-containing groups of carbons and the weak basic sites of zirconia nanoparticles, which can further promote the C–H activation of the ethyl group and electron-donating processes for the catalytic reaction. Simultaneously,

the basic sites also favor the desorption of the styrene molecules from the catalyst surface. In addition, the relatively high BET surface area and open pore channels of the ordered mesoporous ZC-I-600 composite is another important factor for its high catalytic activity.

4. Conclusions

Ordered mesoporous nanocrystalline zirconia/FDU-15 composites have been successfully synthesized by using zirconium oxychloride octahydrate and resol as precursors and Pluronic F127 as a structure-directing agent *via* an EISA approach. The ZrO_2/FDU-15 nanocomposites possess an ordered 2-D hexagonal (*p6mm*) mesostructure, high thermal stability (up to 900 °C), narrow pore size distributions, high specific BET surface areas (up to 910 m^2 g^{-1}), tailorable zirconia content (up to 47 wt%), and small particle size (1.9–3.9 nm) of tetragonal crystalline zirconia confined in the matrices of amorphous carbon pore walls. The degree of pore blocking is very small despite the high embedded amount of zirconia in the carbon pore walls. The successful preparation is mainly due to the co-assembly of resol, zirconium polyoxo species and F127 copolymer driven by the hydrogen-bonding interaction. The obtained mesoporous composites exhibit high catalytic performance with 59.6% of ethylbenzene conversion and 90.4% of styrene selectivity at low temperature of 350 °C, O_2/EB molar ratio of 0.5, and total space velocity of 24 900 mL g^{-1} h^{-1}. The excellent catalytic performance is mainly related to the synergetic interaction between the oxygen-containing groups and weak basic sites of zirconia nanoparticles and its high BET surface area and open pore channels.

Acknowledgements

This work was supported by NSF of China (2089012, 20721063, 20821140537, 20871030), State Key Basic Research Program of PRC (2006CB932302, 2009AA033701), and Shanghai Leading Academic Discipline Project (B108).

References

1 K. Shimizu, I. Chinzei, H. Nishiyama, S. Kakimoto, S. Sugaya, H. Yokoi and A. Satsuma, *Sens. Actuators B*, 2008, **134**, 618.
2 V. V. Plashnitsa, T. Ueda, P. Elumalai and N. Miura, *Sens. Actuators B*, 2008, **130**, 231.
3 K. Yamahara, T. Z. Sholklapper, C. P. Jacobson, S. J. Visco and L. C. de Jonghe, *Solid State Ionics*, 2005, **176**, 1359.
4 H. C. Yao and Y. F. Y. Yao, *J. Catal.*, 1984, **86**, 254.
5 J. Kašpar, P. Fornasiero and N. Hickey, *Catal. Today*, 2003, **77**, 419.
6 K. Tanabe and T. Yamaguchi, *Catal. Today*, 1994, **20**, 185.
7 S. F. Audry, P. E. Hoggan, J. Saussy, J. C. Lavalley, H. Lauron-Pernot and A. M. Le Govic, *J. Catal.*, 1997, **168**, 471.
8 H. Chen, J. Gu, J. Shi, Z. Liu, J. Gao, M. Ruan and D. Yan, *Adv. Mater.*, 2005, **17**, 2010.
9 M. S. Wong and J. Y. Ying, *Chem. Mater.*, 1998, **10**, 2067.
10 H.-R. Chen, J.-L. Shi, W.-H. Zhang, M.-L. Ruan and D.-S. Yan, *Chem. Mater.*, 2001, **13**, 1035.
11 S.-Y. Chen, L.-Y. Jang and S. J. Cheng, *J. Phys. Chem. B*, 2006, **110**, 11761.
12 M. S. Wong, H. C. Huang and J. Y. Ying, *Chem. Mater.*, 2002, **14**, 1961.
13 S.-Y. Chen, L.-Y. Jang and S. Cheng, *Chem. Mater.*, 2004, **16**, 4174.
14 X.-R. Chen, Y.-H. Ju and C.-Y. Mou, *J. Phys. Chem. C*, 2007, **111**, 18731.
15 C. K. Krishnan, T. Hayashi and M. Ogura, *Adv. Mater.*, 2008, **20**, 2131.
16 M. V. Landau, L. Titelman, L. Vradman and P. Wilson, *Chem. Commun.*, 2003, 594.
17 Y. Wang, K.-Y. Lee, S. Choi, J. Liu, L.-Q. Wang and C. H. F. Peden, *Green Chem.*, 2007, **9**, 540.
18 F. Zhang, Y. Meng, D. Gu, Y. Yan, C. Yu, B. Tu and D. Y. Zhao, *J. Am. Chem. Soc.*, 2005, **127**, 13508.
19 Y. Meng, D. Gu, F. Zhang, Y. Shi, H. Yang, Z. Li, C. Yu, B. Tu and D. Y. Zhao, *Angew. Chem. Int. Ed.*, 2005, **44**, 7053.
20 Y. Huang, H. Cai, T. Yu, F. Zhang, F. Zhang, Y. Meng, D. Gu, Y. Wan, X. Sun, B. Tu and D. Y. Zhao, *Angew. Chem., Int. Ed.*, 2007, **46**, 1089.
21 C. You, X. Xu, B. Tian, J. Kong, D. Y. Zhao and B. Liu, *Talanta*, 2009, **78**, 705.
22 Y. Zhu, E. Kockrick, S. Kaskel, T. Ikoma and N. Hanagata, *J. Phys. Chem. C*, 2009, **113**, 5998.
23 Y. Wan, H. Wang, Q. Zhao, M. Klingstedt, O. Terasaki and D. Y. Zhao, *J. Am. Chem. Soc.*, 2009, **131**, 4541.
24 D. Y. Zhao, J. Feng, Q. Huo, N. Melosh, G. H. Fredickson, B. F. Chmelka and G. D. Stucky, *Science*, 1998, **279**, 548.
25 R. Liu, Y. Shi, Y. Wan, Y. Meng, F. Zhang, D. Gu, Z. Chen, B. Tu and D. Y. Zhao, *J. Am. Chem. Soc.*, 2006, **128**, 11652.
26 Y. Wan and D. Y. Zhao, *Chem. Rev.*, 2007, **107**, 2821.
27 J. Xu, L.-C. Wang, Y.-M. Liu, Y. Cao, H.-Y. He and K.-N. Fan, *Catal. Lett.*, 2009, **133**, 307.
28 G. Mestl, N. I. Maksimova, N. Keller, V. V. Roddatis and R. Schlögl, *Angew. Chem., Int. Ed.*, 2001, **40**, 2066.
29 F. Cavani and F. Trifiro, *Appl. Catal. A*, 1995, **133**, 219.
30 F. M. Bautista, J. M. Campelo, D. Luna, J. M. Marinas, R. A. Quirós and A. A. Romero, *Appl. Catal. B*, 2007, **70**, 611.
31 L. Wang, J. Zhang, D. S. Su, Y. Ji, X. Cao and F.-S. Xiao, *Chem. Mater.*, 2007, **19**, 2894.
32 J. J. Delgado, D. S. Su, G. Rebmann, N. Keller, A. Gajovic and R. Schlögl, *J. Catal.*, 2006, **244**, 126.
33 A. Rinaldi, J. Zhang, J. Mizera, F. Girgsdies, N. Wang, S. B. A. Hamid, R. Schlögl and D. S. Su, *Chem. Commun.*, 2008, 6528.
34 B. Nigrovski, U. Zavyalova, P. Scholz, K. Pollok, M. Müller and B. Ondruschka, *Carbon*, 2008, **46**, 1678.
35 J.-N. Park, J. Noh, J.-S. Chang and S.-E. Park, *Catal. Lett.*, 2000, **65**, 75.
36 N. Keller, N. I. Maksimova, V. V. Roddatis, M. Schur, G. Mestl, Y. V. Butenko, V. L. Kuznetsov and R. Schlögl, *Angew. Chem., Int. Ed.*, 2002, **41**, 1885.
37 T.-J. Zhao, W.-Z. Sun, X.-Y. Gu, M. Rønning, D. Chen, Y.-C. Dai, W.-K. Yuan and A. Holmen, *Appl. Catal. A*, 2007, **323**, 135.